

DIAS: A Comprehensive Benchmark for DSA-sequence Intracranial Artery Segmentation

Wentao Liu¹, Tong Tian³, Lemeng Wang¹, Weijin Xu¹, Haoyuan Li¹, Wenyi Zhao¹, Xipeng Pan⁵, Huihua Yang^{1,5,*}, Feng Gaog^{2,*}, Yiming Deng², Ruisheng Su⁴

¹*School of Artificial Intelligence, Beijing University of Posts and Telecommunications, Beijing 100876, China*

³*Department of Interventional Neuroradiology, Beijing Tiantan Hospital, Capital Medical University, Beijing, 100070, China*

²*State Key Laboratory of Structural Analysis, Optimization and CAE Software for Industrial Equipment, School of Aeronautics and Astronautics, Dalian University of Technology, Dalian 116024, China*

⁴*School of Computer Science and Information Security, Guilin University of Electronic Technology, Guilin 541004, China*

⁵*Department of Radiology & Nuclear Medicine, Erasmus MC, University Medical Center Rotterdam, The Netherlands*

liuwentao@bupt.edu.cn

Abstract—Automatic segmentation of the intracranial artery (IA) in digital subtraction angiography (DSA) sequence is an essential step in diagnosing IA-related diseases and guiding neuro-interventional surgery. However, the lack of publicly available datasets has impeded research in this area. In this paper, we release DIAS, an IA segmentation dataset, consisting of 120 DSA sequences from intracranial interventional therapy. In addition to pixel-wise annotations, this dataset provides two types of scribble annotations for weakly supervised IA segmentation research. We present a comprehensive benchmark for evaluating the performance of this challenging dataset by utilizing fully-, weakly-, and semi-supervised learning approaches. Specifically, we propose a method that incorporates a dimensionality reduction module into a 2D/3D model to achieve vessel segmentation in DSA sequences. For weakly-supervised learning, we propose a scribble learning-based image segmentation framework, SSCR, which comprises scribble supervision and consistency regularization. Furthermore, we introduce a random patch-based self-training framework that utilizes unlabeled DSA sequences to improve segmentation performance. Our extensive experiments on the DIAS dataset demonstrate the effectiveness of these methods as potential baselines for future research and clinical applications. The dataset and code will be publicly available at <https://github.com/lseventeen/DIAS>.

Index Terms—digital subtraction angiography, intracranial artery segmentation, dataset, semi-supervision learning, weakly supervision learning

I. INTRODUCTION

IN the last few decades, the mortality rate of intracranial artery (IA) diseases, such as intracranial arterial stenosis (ICAS), middle cerebral artery occlusion (MCAO), and intracranial aneurysm, has significantly decreased, thanks to rapid advancements in medical imaging technology [1]. Among all medical imaging techniques, digital subtraction angiography (DSA) is widely regarded as the gold standard

for exploring lesion angioarchitecture, understanding arterial blood supply dynamics, and providing unique endovascular treatments [2]. Given its inherently high spatial and temporal resolution, DSA can accurately display the lesion details while computed tomography angiography (CTA) and magnetic resonance angiography (MRA) fail to make a clear diagnosis [1]. Accurate segmentation of contrast-filled vessels from the DSA sequence is an essential step for the diagnosis and treatment of IA disease. Currently, DSA-based cerebrovascular image segmentation is applied in clinical practice, including automated thrombolysis in cerebral infarction scoring [3], [4], 3D reconstruction of vessel [5], and image guidance of interventional surgery [6].

DSA is an imaging technique that captures a sequence of images showing the flow of a contrast agent through vessels, with the recording usually lasting 3 to 15 seconds and a sampling rate of 3 to 5 frames per second [7]. Although the images generated by removing bony structures through digital subtraction only show intravascular contrast, developing automated vessel segmentation on DSA sequence is still a challenging task. The challenges arise from various factors, including arteries overlapping and intertwining in projection images, low contrast in thin vessels, as well as the presence of complex and dynamic background artifacts. In the past few years, deep learning has demonstrated great potential in vessel segmentation, surpassing traditional methods, such as hand-crafted features [8], filtering-based models [9], and statistical models [10]. Although several deep learning-based methods for DSA vessel segmentation have emerged, they are mostly developed on private datasets and follow the traditional approach of segmenting each 2D image separately [11], [12]. In reality, the 2D DSA sequence displays a projection of intravascular contrast media at the same viewing angle, as shown in Fig. 1, visualizing only part of IA within the contrast agent in a single image. Hence, 2D DSA segmentation methods cannot fully capture the vascular information of IA and may

This work was supported in part by the National Key Research and Development Program of China under Grant 2018AAA0102600 and in part by the National Natural Science Foundation of China under Grant 62002082.

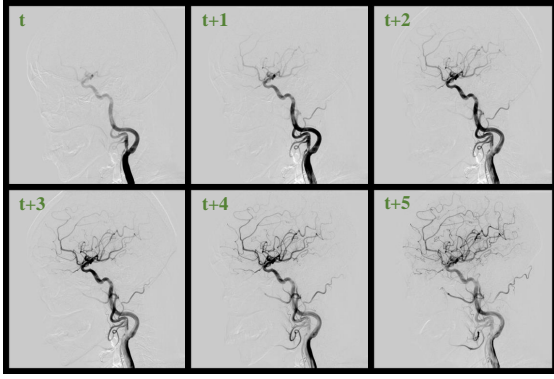


Fig. 1. A representative sample of intracranial vessels in sagittal view from DSA, where t to $t+5$ are consecutive frames of the arterial phase.

be inadequate for diagnosis and treatment of cerebrovascular diseases.

The imaging modality of DSA sequences demands IA segmentation to be considered a dimensionality-reduction segmentation task with 2D+time image input and 2D mask output. Successful segmentation of IA in DSA heavily depends on the exploitation of angiography information available in image sequences. However, there is a lack of research on DSA-sequence vessel segmentation. Furthermore, there is currently no publicly available DSA dataset for IA segmentation in the medical imaging community. Our observation indicates that several factors may account for this phenomenon. First, CTA and MRA have replaced DSA, an invasive examination technology, as the primary means of IA disease examination due to technological advancements. As a result, most of the available DSA data are obtained from interventional therapy, and these data are difficult to acquire. Second, the complex structure of IA in DSA images, with an intricate interwoven of many thin vessels, increases the annotation workload for neurologists significantly.

To address these issues, we construct **DIAS**, a **DSA**-sequence **Intracranial Artery Segmentation** dataset. The DSA sequence has been pixel-level annotated by neurosurgeons. Moreover, since the work of vessel annotation in DSA sequences is extremely tedious and time-consuming, we performed two forms of weak annotation on training samples to facilitate studies on weakly-supervised IA segmentation. For DIAS, we designed three benchmarks for fully-supervised segmentation (FSS), weakly-supervised segmentation (WSS), and semi-supervised segmentation (SSS) methods, considering DIAS’s imaging and annotation format: the 2D/3D model combined with the dimensionality reduction module, the scribble learning-based segmentation framework SSCR and the random patch-based self-training framework. We believe that DIAS will significantly shed light on researchers, especially those without a medical background, in delving into the DSA-sequence vessel segmentation method.

II. RELATED WORK

A. Vessel Segmentation Datasets

Vessel segmentation is a popular area of research within computer-aided medicine, which has witnessed remarkable

progress in recent years, owing to technological advancements and the availability of high-quality annotated datasets. We have summarized the publicly available vessel segmentation datasets in Table I. A representative example is retinal vessel segmentation, which has many publicly available datasets due to its easy availability, such as colour fundus datasets (DRIVE [13], CHASE_DB1 [14], STARE [15], HRF [16]) and OCTA datasets (ROSE1 and ROSE2 [17]). These datasets consist of 2D images with numbers ranging from 20 to 117 and resolutions ranging from 304×304 to 3504×2336 . However, other vessel segmentation datasets are relatively scarce. CHUAC [18] and DCA1 [19] are coronary angiography datasets with resolutions of 189×189 and 300×300 , respectively. ASOCA [20] and VESSEL12 [21] are the 3D vessel segmentation datasets of coronary artery CTA and lung CT from the challenges, in which only training set data is available. The availability of such datasets has led to a surge of outstanding works in the field of segmentation, with researchers striving to develop algorithms that outperform existing methods. Thus far, there have been no publicly available DSA datasets with vessel annotation in the medical imaging community, and only a few studies conducted with in-house datasets. DCVessel [11] comprises 30 DSA arterial-phase images at a resolution of 700×700 , while HEART [22] comprises 1092 DSA coronary images at 256×256 resolution. We present the DSA-sequence IA segmentation dataset (DIAS), which can serve as a reliable benchmark for the development of algorithms on IA segmentation. We hope that this dataset will intrigue researchers to explore this field further.

B. Vessel Segmentation Methods

In recent years, deep learning-based methods have become primary approaches for vessel segmentation, with UNet [23] serving a crucial role as a milestone network architecture. Developed as a convolutional neural network (CNN), derivatives of UNet have been widely used in various segmentation tasks, providing better performance than traditional methods [24]. These networks utilize an encoder-decoder architecture with popular components, such as multi-scale design [11], [25], [26], deep supervision [11], [27], [28], attention mechanisms [25], [29], [30], atrous convolution [11], [27], [28], [31], and improved skip connections [11], [28]. Moreover, several novel neural networks [32], [33] have also succeeded in vessel segmentation by leveraging generative adversarial networks (GAN) or graph neural networks (GNN). Some studies focused on vessel segmentation beyond network architecture, such as optimized training strategies [34], [35] and modifying loss functions [36]. However, there have been few studies on DSA vessel segmentation. Meng *et al.* [11] proposed a CNN-based multiscale dense CNN segmentation framework, which includes a multiscale atrous convolution module, an improved dense block, and redesigned skip connections, for IA segmentation in single frame DSA. Zhang *et al.* [22] proposed a boundary enhancement and feature denoising module to improve the network’s ability to extract boundary information in DSA coronary segmentation. These two methods, developed on in-house DSA datasets as fully-supervised segmentation

TABLE I
PUBLIC VESSEL SEGMENTATION DATASETS. † REPRESENTS ONLY
TRAINING SET DATA IS AVAILABLE.

Dataset	Organ	Modality	Type	Dimension	Resolution
DRIVE [13]	retina	color fundus	2D	40	565×584
CHASE_DB1 [14]	retina	color fundus	2D	28	999×960
STARE [15]	retina	color fundus	2D	20	700×605
HRF [16]	retina	color fundus	2D	45	3504×2336
ROSE1 [17]	retina	OCTA	2D	117	304×304
ROSE2 [17]	retina	OCTA	2D	112	512×512
CHUAC [18]	coronary artery	angiography	2D	30	189×189
DCA1 [19]	coronary artery	angiography	2D	134	300×300
ASOCA* [20]	coronary artery	CTA	3D	40	512×512×200
VESSEL12* [21]	lung vessel	CT	3D	20	-
DIAS (ours)	intracranial artery	DSA	2D+Time	60+60	800×800×8

methods, are only applicable for vessel segmentation in single frame DSA and cannot be used for DSA sequences. To our knowledge, there is no existing literature on semi-supervised or weakly-supervised vessel segmentation in DSA sequences. In this regard, we propose a comprehensive benchmark involving FSS, WSS, and SSS for IA segmentation based on the constructed DSA-sequences dataset.

III. DIAS DATASET

A. Dataset Description

The DIAS dataset was derived from intraoperative DSA images obtained during ICAS and MCAO treatments at Beijing Tiantan Hospital. The ethical committee at Beijing Tiantan Hospital authorized the use of all the data presented in this study. All images were retrospectively collected between January 2019 and December 2021 and then anonymized to protect the patients' privacy by removing all identifiable clinical treatment details. A total of 60 patients (120 cases) were included in the dataset, of whom 24 were female and 36 were male, with a mean age of 62.5 years, ranging from 40 to 88 years old. Each patient's data contains at least one DSA sequence capturing the intracranial arterial phase and located in either the coronal or sagittal view. The original DSA sequences were captured by the angiography machine during the actual endovascular therapy process and stored as DICOM files. The number of frames varied across different sequences, ranging from 6 to 46 frames. The sequences were then extracted into individual images with a resolution of 800×800 pixels using MicroDicom. We retained all the arterial-phase frames and removed the pre-contrast, capillary-phase, and venous-phase frames under the guidance of a neurosurgeon. As a result, the length of DSA sequences in the DIAS dataset ranges from 4 to 11 frames. To facilitate input into the model, all DSA sequences were resampled to a length of 8. Each sequence had a final dimension of 800×800×8.

B. Reference Annotation Protocol

1) *Full Annotation*: Manual annotation of IA in DSA sequences requires taking into account all the image information in the sequence. Fig. 1 shows an example of intracranial

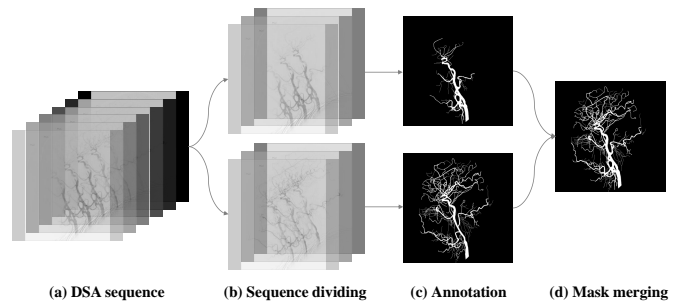


Fig. 2. Full annotated process of DIAS.

vessels in five consecutive frames of the arterial phase in the sagittal view. During this period, the contrast agent is gradually dispersed from the internal carotid artery (ICA) to cerebral vessels such as the anterior cerebral artery (ACA), middle cerebral artery (MCA), and posterior cerebral artery (PCA) with blood flow. For a single image, the contrast agent is visible only in a portion of the IA. For instance, the contrast agent at t filled the C1-C3 segment of the ICA, while at $t+4$, it filled the ACA, MCA, and PCA. Annotating the IA of each image in the sequence and then merging the annotation mask can maximize the utilization of the sequence's vessel information to obtain accurate annotations. The thinness of vessels, particularly in later-stage arterial images, renders the commonly used strategy of outlining their borders in medical image annotation unfeasible. Thus, we have to annotate each vessel pixel by pixel, which is a labor-intensive and time-consuming procedure. Fig. 3 shows that our proposal for a compromise solution, which reduces workload while maintaining annotation accuracy:

- 1) The arterial-phase DSA sequences were divided into two phases from the middle: the anterior phase and the later phase. The contrast agent during the anterior phase predominantly fills the ICA as opposed to the smaller vessels such as the ACA, MCA, and PCA arteries, which are filled by the contrast agent in the later phase.
- 2) The last image of each phase is annotated pixel-wise, followed by a meticulous review of other same-phase images to finalize the annotation. Thick vessels are the focus of annotation in the anterior phase, while thin vessels are prioritized in the later phase.
- 3) The annotations of thick and thin vessels are merged using a pixel-level OR operation (1 for vessel pixel and 0 for background) to create the ultimate vessel mask.

We randomly selected 60 sequences from DIAS for sequence annotation based on patient ID. The remaining 60 sequences were used for research on IA semi-supervised segmentation. The DSA sequence was initially annotated by two MD students of surgery, followed by corrections from an associate physician with 10 years of experience, and finally confirmed and double-checked by a chief physician with 15 years of experience.

2) *Scribble Annotation*: Scribble-based image segmentation has proven to be an efficacious and sought-after method for WSS [37]. This approach to weak annotation allows annotators to easily mark object centers without the chal-

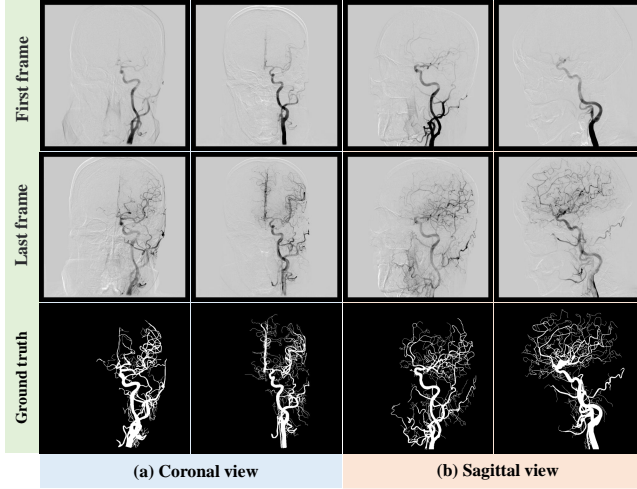


Fig. 3. Full annotated representative samples of DIAS at coronal view and sagittal view.

lenging task of delineating class boundaries. To explore the potential of scribble supervision for IA segmentation in DSA sequences, we generated two forms of scribble annotations for the training set of DIAS: the Scribbles Annotation with Little Clinical Experience (SALE) and the Drawing Centerlines Randomly (DCR). SALE simulates vessel annotation with little expert experience, wherein the thick vessels highlighted by the contrast agent are annotated, as shown in Fig. 4 (a). DCR is a type of scribble annotation where the centerline is randomly drawn [38], as shown in Fig. 4 (b). Despite receiving clinicians’ basic training, accurately distinguishing the thin vessels and edges of thick blood vessels with low contrast and complex structures remains challenging. Consequently, pixels in these regions were unmarked during annotation. Remarkably, SALE is able to mark a sequence in only 1/8 of the time required for a full annotation.

IV. METHODS

Automatic IA segmentation in DSA sequences is an under-explored and challenging task. To fully explore potential research topics, three elaborately designed benchmarks for IA segmentation were proposed, aiming to provide comprehensive benchmarks for FSS, WSS, and SSS, which are increasingly drawing attention in the medical image analysis community.

A. Fully-supervised Segmentation

Segmenting IA in DSA sequence can be considered as a dimensionality reduction (DR) task. Given an image $I \in \mathbb{R}^{\prod_{d=1}^N n_d}$, where N represents the number of dimensions and n_d is the size of the image in the corresponding dimension d , DR segmentation can be defined as finding a function f such that $f : I \rightarrow O$, where $O \in \mathbb{R}^{\prod_{d=1}^M n_d}$ represents segmentation output and $M (< N)$ is its dimensionality [39]. For IA segmentation in DSA sequence, $N = 3$, $M = 2$. Although several approaches have been proposed to deal with DR in segmentation tasks [39], [40], they employ DR operations in the encoder or decoder of the model, which may not

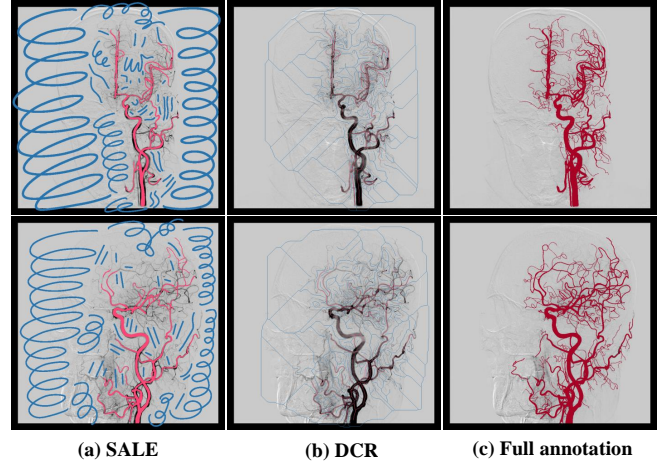


Fig. 4. Examples of two forms scribble annotations: the scribbles annotation with little clinical experience (SALE) and drawing centerlines randomly (DCR). Red represents annotated vessel pixels, blue represents annotated background pixels.

be applicable to all segmentation models. In our previous work [25], [41], [42], 2D and 3D models were proposed for the segmentation of retinal vessels and aortas, converting them to the DR model is laborious and could potentially disrupt the structure of the model.

To tackle this issue, we propose a straightforward yet efficient DR module that can convert typical 2D and 3D segmentation models into DR models without altering their design. As shown in Fig. 5 (a), the DR module (DRM) is readily integrated into the input of a 2D model or the output of a 3D model as a plug-and-play module. Specifically, given a DSA sequence $x \in \mathbb{R}^{C \times F \times H \times W}$, where C , F , H and W denote the number of channels, frame, height, and width, respectively. The initial number of channels is 1, which is squeezed by DRM. The compressed input is then fed to the 2D model, where F replaces C as the input channel:

$$y = \mathcal{H}_{2d}(\text{Squ}(x)) \quad (1)$$

where, Squ is dimensionality squeeze operation and \mathcal{H}_{2d} is a 2D model.

For a 3D model \mathcal{H}_{3d} , the DSA sequence is fed directly into the model, where it is treated as volume data. The dimension, C , of the model output is squeezed by DRM. Finally, 1×1 convolution reduces F to the number of classes:

$$y = \text{Conv}_{1 \times 1}(\text{Squ}(\mathcal{H}_{3d}(x))) \quad (2)$$

B. Weakly-supervised Segmentation

A common strategy for scribble-supervised semantic segmentation is to handle the problem as a fully supervised task, using a loss function \mathcal{L} on the available labeled points. However, this baseline approach does not utilize the unlabeled points that contain critical semantic information. The performance degradation is unavoidable due to the lack of labeled data points. To enhance the segmentation performance of scribble, the key lies in extending the supervision of

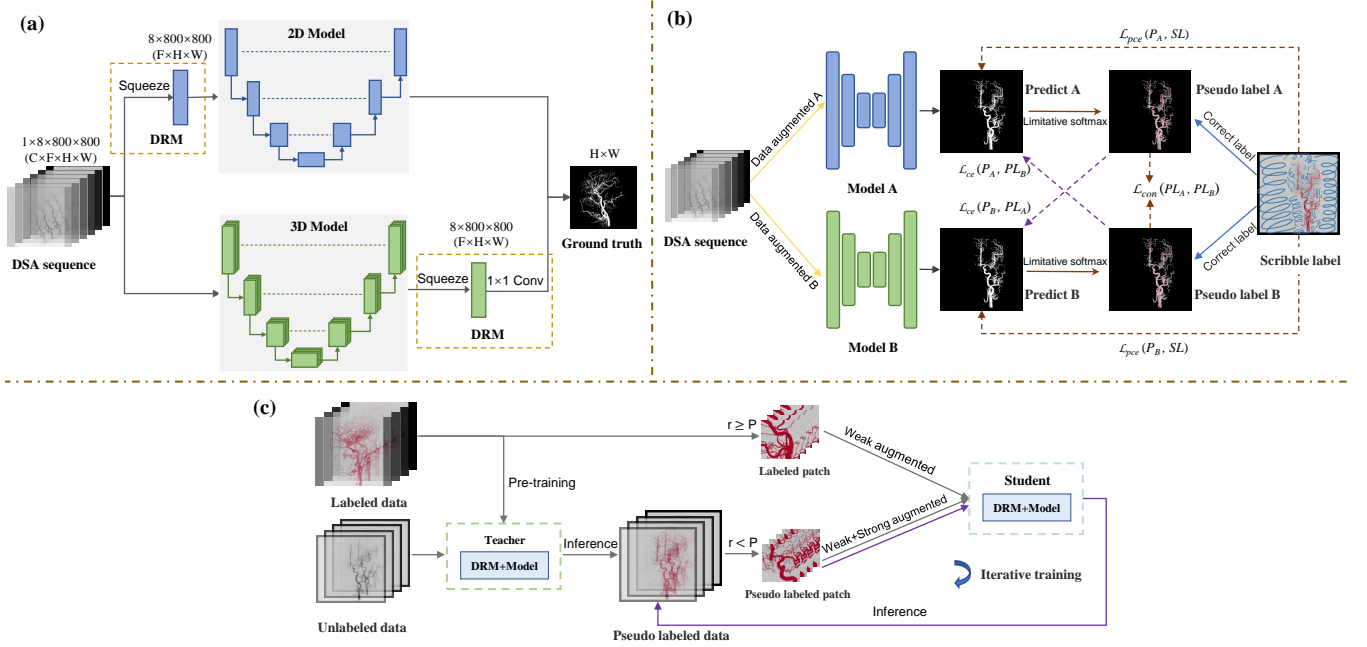


Fig. 5. Illustration of the proposed pipeline for intracranial artery segmentation in DSA, comprising three learning-based methods (a) Fully-supervised learning: embedding the dimensionality reduction module outside the 2D/3D model; (b) Weakly-supervised learning: scribble learning-based segmentation composed of scribble supervision and consistency regularization; (c) Semi-supervised learning: random patch-based self-training framework.

labeled pixels to unlabeled pixels. To overcome these issues, we propose SSCR, a novel framework for learning-based scribble image segmentation composed of scribble supervision and consistency regularization. Fig. 5 (b) presents the implementation framework for SSCR. SSCR generates pseudo-annotations for the unlabeled pixels with guidance provided by scribble supervision, utilizing partial cross-entropy to extend supervised information, and maximizes the performance of scribble segmentation by regularizing segmentation network using mutual consistency and cross pseudo supervision.

We define P as the set of image pixels and $S \subseteq P$ as the set of annotated pixels. The proposed approach feeds P into two segmentation networks with different augmentation strategies. The outputs of each network are supervised by applying the cross-entropy function solely to the annotated pixels on the scribble labels. The function, namely partial cross entropy, can be formulated as:

$$\mathcal{L}_{pce}(y, \hat{y}) = \sum_{i=1}^P \sum_{j=1}^C \mathbb{1}(p_i \in S) (-y_{i,j} \log(\hat{y}_{i,j}|\theta)) \quad (3)$$

where, $\hat{y}_{i,j}|\theta$ is the predict on class $j \in C$ for the pixel $p_i \in P$ given the network parameters θ , and $y_{i,j}$ denotes the ground truth label.

To generate pseudo labels, we first calculate the class distribution of the one-hot prediction map using limited softmax, which solely accounts for the channel of the labeled class. Then, we apply scribble annotations to correct the pseudo labels in order to improve their confidence. The formula for creating the pseudo label is as follows:

$$PL_i = \begin{cases} s_i, & \text{if } p_i \in S \\ \text{argmax}(\text{softmax}(\mathcal{H}(p_i; \theta)[: C])), & \text{otherwise} \end{cases} \quad (4)$$

where, $s_i \in S$ defines annotated pixels, and $\mathcal{H}(p_i; \theta)$ defines the predicted output of p_i . C is the number of classes.

We enforce network consistency by utilizing cross pseudo-supervision, which employs pseudo labels from one network to supervise the other network [43]. Additionally, these pseudo labels are imposed a consistency loss to penalize inconsistent segmentation. The training objective contains three losses: scribble supervision loss \mathcal{L}_{scr} , cross pseudo supervision loss \mathcal{L}_{cps} , and consistency loss \mathcal{L}_{con} :

$$\begin{aligned} \mathcal{L}_{scr} &= \frac{1}{2} (\mathcal{L}_{pce}(P_A, SL) + \mathcal{L}_{pce}(P_B, SL)) \\ \mathcal{L}_{cps} &= \frac{1}{2} (\mathcal{L}_{ce}(P_A, PL_B) + \mathcal{L}_{ce}(P_B, PL_A)) \\ \mathcal{L}_{con} &= \mathcal{L}_{mse}(PL_A, PL_B) \end{aligned}$$

where, \mathcal{L}_{ce} denotes the cross-entropy loss function and \mathcal{L}_{mse} denotes the mean square error loss function. P_A and P_B are the outputs of two models. PL_A and PL_B are the pseudo labels. SL is the scribble label.

Finally, the training objective \mathcal{L} is formulated as

$$\mathcal{L} = \mathcal{L}_{scr} + \lambda_1 \mathcal{L}_{cps} + \lambda_2 \mathcal{L}_{con} \quad (5)$$

where, λ_1 and λ_2 are the weight of loss components \mathcal{L}_{cps} and \mathcal{L}_{con} .

C. Semi-supervised Segmentation

Annotation of cerebral vessels manually from DSA image sequences is a laborious and time-consuming task. Semi-supervised learning has shown the potential to alleviate this problem by learning from a large set of unlabeled images and limited labeled samples [44]. The primary challenge in semi-supervised setting lies in how to effectively utilize the

unlabeled images. Self-training [45] via pseudo labeling is a conventional, simple, and popular pipeline to leverage unlabeled data, where the retrained student is supervised with hard labels produced by the teacher trained on labeled data, which is commonly regarded as a form of entropy minimization in semi-supervised learning. For semi-supervised segmentation problem, let $\mathcal{D}^l = \{(x_i, y_i)\}_{i=1}^M$ be pixel-wise labeled images and $\mathcal{D}^u = \{u_i\}_{i=1}^N$ be unlabeled images, where in most cases $N \gg M$. Self-training can be simplified into the following steps:

- 1) Train a teacher model T on labeled data \mathcal{D}^l ;
- 2) Predict hard pseudo labels on unlabeled data \mathcal{D}^u with T to obtain $\hat{\mathcal{D}}^u = \{(u_i, T(u_i))\}_{i=1}^N$;
- 3) Re-train a student model S on the label data and pseudo-label data $\mathcal{D}^l \cup \hat{\mathcal{D}}^u$ for final evaluation.

We follow the plainest self-training strategy to provide a SSS benchmark for DIAS. The injection of strong data augmentations on unlabeled images is highly advantageous as it decouples the predictions as well as alleviates overfitting on noisy pseudo-labels. Despite its simplicity, self-training with strong data augmentations surpasses existing methods without any bells and whistles [46]. We performed two types of data augmentations in our implementation: weak and strong, denoted by A^s and A^w respectively. Weak data augmentations consist of horizontal flipping, vertical flipping, and [90, 180, 270] degree rotation. Strong data augmentations include Cutout, adding white Gaussian noise, Gaussian blurring, and elastic deformation. We randomly adjust the contrast of each image in the DSA sequence to simulate angiography with intensity differences. We randomly extract patches from the DSA sequence to train the teacher and student models. Notably, the patches in each mini-batch were randomly extracted from \mathcal{D}^l and $\hat{\mathcal{D}}^u$ with a probability P when retraining the student model. Additionally, the final performance can be further improved by switching the teacher-student role and relabeling unlabeled images for iterative training. The pseudocode of the random patch-based self-training framework, referred to as pST, is provided in Algorithm 1.

V. EXPERIMENTS AND RESULTS

A. Implementation Details and Evaluation Metrics

The DIAS dataset was divided into 30 training samples, 10 validation samples, and 20 testing samples on the patient level. All DSA sequences were z-score normalized. Patches of size $8 \times 64 \times 64$ were randomly cropped for training, with a batch size of 64. The model parameters were optimized using AdamW [47] with an initial learning rate of $5e-4$. The learning rate is gradually reduced by the cosine annealing algorithm over 100 epochs. We selected ‘DRM+2D FR-UNet’ as the teacher and student of pST, and as the model of SSCR due to its outstanding performance as demonstrated in Sec V-B. The parameter P was set to 0.5, i.e., half of the patches in each batch were extracted from labeled data, while the rest came from unlabeled data in SSS experiment. The weights of loss components λ_1 and λ_2 were empirically set to 1 and 0.5 for SSCR. All experiments used PyTorch with constant hyperparameters and were conducted on a single

Algorithm 1: pST

Input: Labeled training set $\mathcal{D}^l = \{(x_i, y_i)\}_{i=1}^M$,
 Unlabeled training set $\mathcal{D}^u = \{u_i\}_{i=1}^N$,
 Weak/strong augmentation $\mathcal{A}^w/\mathcal{A}^s$,
 Teacher/student model T/S ,
 Execution probability $P \in (0, 1)$

Output: Trained student model S

Train T on \mathcal{D}^l with loss \mathcal{L}

Obtain pseudo labeled $\hat{\mathcal{D}}^u = \{(u_i, T(u_i))\}_{i=1}^N$

for minibatch with the size of B **do**

for $k \in \{1, \dots, B\}$ **do**

if Random number $r > P$ **then**

 Randomly extract patch (x_k^p, y_k^p) from \mathcal{D}^l

$x_k^p, y_k^p \leftarrow (\mathcal{A}^s \& \mathcal{A}^w)(x_k^p, y_k^p)$

else

 Randomly extract patch (x_k^p, y_k^p) from $\hat{\mathcal{D}}^u$

$x_k^p, y_k^p \leftarrow \mathcal{A}^w(x_k^p, y_k^p)$

end

$\hat{y}_k^p = S(x_k^p)$

 Update S to minimize \mathcal{L} of $\{(\hat{y}_i^p, y_k^p)\}_{i=1}^B$

end

Obtain new pseudo labeled $\hat{\mathcal{D}}^u = \{(u_i, S(u_i))\}_{i=1}^N$ for iterative training

GeForce RTX 3090 GPU. We calculated the dice similarity coefficient (DSC), the area under the receiver operating characteristic curve (AUC), accuracy (Acc), sensitivity (Sen), specificity (Spe), and intersection over union (IOU) to evaluate the performance of DSA sequence segmentation. Moreover, we introduced the vascular connectivity (VC) [41] metric, which calculates the ratio of connected components in the segmentation image to those in the ground truth, as a means of measuring the connectivity of vessels.

B. Fully-supervised Segmentation

We employed DRM in 2D/3D models to achieve DSA sequence segmentation. To validate this approach, we performed experiments on DIAS using seven state-of-the-art segmentation models, which included 2D and 3D models such as UNet [23], Attention-UNet [48], UNet++ [49], Res-UNet [50], MAA-Net [25], CS²Net [29], and FR-UNet [41]. Additionally, we compared two 3D→2D models proposed for OCTA segmentation. The Image Projection Network (IPN) [40] utilizes unidirectional pooling for aggregating information from 3D data into a 2D projection plane, yielding accurate 3D→2D image segmentation. To address the inconsistent feature map dimensions, Dmitrii *et al.* [39] propose projective skip-connections (PSC), which allow linking the encoder and decoder in a UNet-like structure.

Table II demonstrates that the comprehensive performance of the ‘DRM+2D model’ slightly outperforms that of the ‘DRM+3D model’. The ‘DRM+2D model’ benefits from treating ‘sequences’ as ‘channels’, which enables it to learn local representations along the sequence dimension while performing 2D convolutions. This approach aggregates contrast agent responses that reflect vascular morphological in-

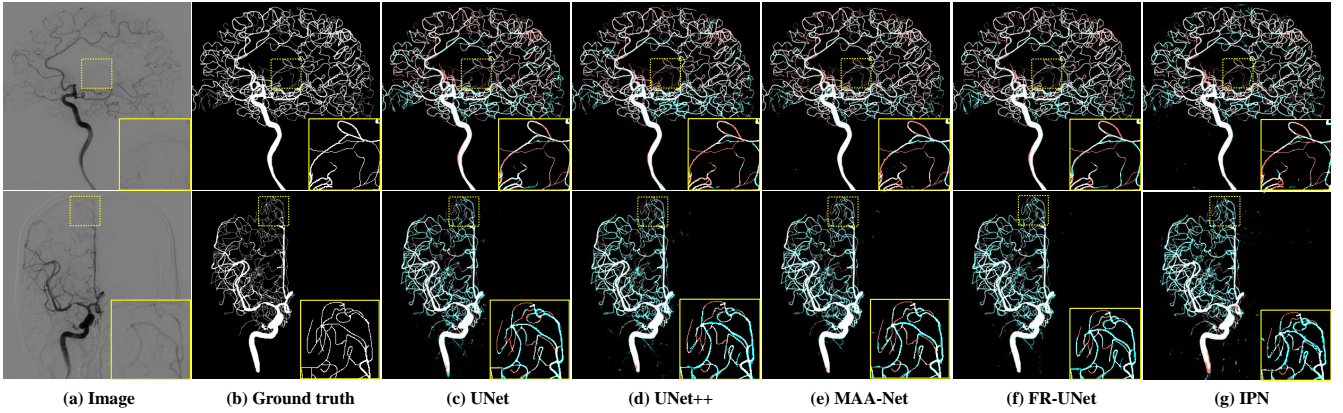


Fig. 6. Visualization of segmentation results of state-of-the-art models. The first row is coronal view, and the second row is sagittal view. The red pixel indicates false positives, and the green pixel indicates false negatives.

TABLE II
RESULTS OF FULLY-SUPERVISED SEGMENTATION WITH
STATE-OF-THE-ART MODELS.

Methods	Params	Metrics							
		DSC	Acc	Sen	Spe	IOU	AUC	VC ↓	
DRM+2D	UNet [23]	31.04	76.57	96.43	75.94	98.27	62.30	98.06	93.11
	Res-UNet [50]	9.37	76.57	96.45	75.73	98.28	62.26	98.03	72.57
	UNet++ [49]	9.05	76.79	96.47	75.97	98.30	62.54	98.07	77.48
	Att-UNet [48]	8.73	77.58	96.62	76.02	98.47	63.60	98.31	68.48
	CS ² Net [29]	8.93	76.88	96.50	75.80	98.35	62.70	98.17	69.28
	MAA-Net [25]	5.80	77.27	96.64	74.50	98.60	63.24	98.21	74.29
	FR-UNet [41]	7.37	78.34	96.71	77.53	98.44	64.60	98.53	52.88
DRM+3D	UNet [23]	90.27	74.50	96.15	73.20	98.16	59.59	97.36	122.13
	Res-UNet [50]	26.38	75.77	96.37	74.08	98.33	61.26	97.73	80.04
	UNet++ [49]	26.17	74.15	96.13	72.62	98.19	59.18	97.29	111.41
	Att-UNet [48]	23.60	75.17	96.27	73.69	98.25	60.49	97.59	91.76
	CS ² Net [29]	23.83	75.27	96.23	74.48	98.13	60.67	97.83	89.20
	FR-UNet [41]	20.57	77.28	96.60	75.67	98.45	63.21	98.34	56.75
3D→2D	IPN [40]	6.36	75.32	96.38	72.56	98.43	60.68	97.28	66.51
	PSC [39]	6.43	75.61	96.32	74.06	98.26	61.04	97.81	75.50

formation in the sequence direction. However, the 3D model underperformed since the sequence dimension of DIAS is much smaller than the other dimensions (H and W). The ‘DRM+2D FR-UNet’ model achieved the highest scores on metrics such as DSC, IOU, AUC, and VC, and ranked second (slightly below MAA-Net and Res-UNet, respectively) on Acc and Sen, among all the evaluated methods. Meanwhile, IPN, a 3D→2D model, performed poorly relative to the other models, primarily because it only reduced the size of the sequence dimension while keeping the image width and height unchanged. Consequently, the receptive field of the learned representation is small, thereby limiting its effectiveness. Fig. 6 shows the segmentation results. The green and red pixels reveal that none of the models can accurately segment small vessels, especially those with only one pixel in width. Under-segmentation and incorrect segmentation remain challenging in vessel segmentation.

C. Weakly-supervised Segmentation

We compared our method with four scribble-supervised segmentation methods: pCE [51], Entropy Minimization (EM) [52], Regularized Loss (RLoss) [37], and Intra-class intensity variance minimization (IVM) [38]. Table III presents the results of scribble-supervised segmentation of the DIAS dataset. Thanks to pseudo supervision and consistency regularization for scribble supervision, SSCR achieved significantly better performance in DCR and SALE by obtaining the highest scores in most metrics among all methods. Fig. 7 showcases the visual results of all methods. In DCR, the red-circled region points out that the artifacts generated by digital subtraction were mis-segmented as vessels. SSCR outperforms other methods by having fewer false positives, as indicated by the area of the cyan pixels independent of the vessel tree. Regarding SALE, the vessels segmented by the same method are thicker than the ones trained with DCR labeling, leading to a larger number of false positive pixels at the vessel’s edge. This outcome was caused by the SALE focusing on the annotation of thick vessels. As evidenced by the third row, the segmentation map of SSCR is closest to ground truth.

We conducted ablation studies to investigate the impact of various components in our proposed pipeline for weakly-supervised IA segmentation. As seen in Table IV, we observe a 0.59% increase in DSC by adding PS with extended limited supervision to unlabeled pixels. Applying CPS at the PS of the dual model further increases the DSC by 0.84% benefits from the mechanism of cross-supervision. Based on this, we employ CR on the pseudo-labels generated by dual models to penalize inconsistent segmentation. The resulting SSCR achieved the highest scores on all metrics, except for Sen, which measures the correct proportion of vessel pixels in the ground truth, without including the background pixels. A high score on Sen may increase false positives and degrade overall performance, as shown by the results of IVM in Fig. 7.

D. Semi-supervised Segmentation

The number of labeled and unlabeled samples and strong data augmentation (SDA) affect the performance of pST. In this section, we randomly select 1, 3, and 10 labeled DSA

TABLE III
RESULTS OF SCRIBBLE-SUPERVISED IA SEQUENCE SEGMENTATION.

Methods	DCR							SALE						
	DSC	Acc	Sen	Spe	IOU	AUC	VC ↓	DSC	Acc	Sen	Spe	IOU	AUC	VC ↓
pCE [51]	74.89	95.92	78.81	97.38	60.04	97.18	43.55	64.34	92.49	86.20	92.98	47.79	96.77	5.65
EM [52]	75.61	96.02	79.71	97.41	61.01	97.79	36.56	63.77	92.20	85.94	92.68	47.30	96.28	8.59
RLoss [37]	74.35	96.23	71.21	98.40	59.34	97.43	37.60	60.84	91.87	80.29	92.82	44.02	95.95	3.81
IVM [38]	73.54	95.49	80.91	96.72	58.38	97.00	40.37	63.31	91.98	88.20	92.27	46.70	96.81	5.57
SSCR	76.61	96.34	77.64	97.91	62.26	97.97	33.88	67.64	93.50	83.00	94.32	51.62	97.10	7.40

TABLE IV
ABLATION STUDIES RESULTS OF SSCR FOR SCRIBBLE-SUPERVISED IA SEQUENCE SEGMENTATION.

Methods				Metrics						
pCE	PS	CPS	CR	DSC	Acc	Sen	Spe	IOU	AUC	VC ↓
✓				74.89	95.92	78.81	97.38	60.04	97.18	43.55
✓	✓			75.48	96.02	79.15	97.46	60.83	97.53	34.90
✓	✓	✓		76.32	96.23	78.94	97.69	61.86	97.86	38.34
✓	✓	✓	✓	76.61	96.34	77.64	97.91	62.26	97.97	33.88

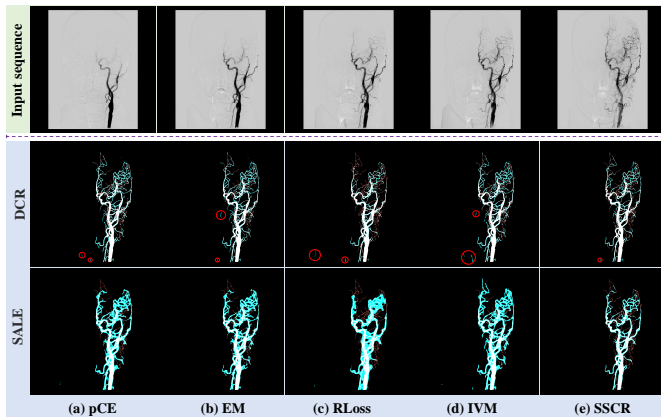


Fig. 7. Visualization of the segmentation results of scribble supervised segmentation methods trained on DCR and SALE annotations.

sequences from the DIAS training set for SSS experiments. We leverage 30 or 60 DSA unlabeled sequences to generate pseudo labels and participate in training student. Table V shows that pseudo-labeled data generated by the trained teacher significantly improves the performance of the model, especially when there are fewer labeled data available. For example, the DSC of the student is improved by 2.89% with one labeled data and 30 unlabeled data compared to the teacher. This performance gain is positively correlated with the amount of unlabeled data. Ablation studies of SDA indicate their effectiveness in promoting the generalization of the model. While the pseudo-labeled data used to train the student model contains noisy labels, they can still enhance the model’s generalization capability, albeit with the supervision of incorrect pixel labels of vessel. The results of DIAS show that the benefits brought by the pseudo-labeled data outweigh the drawbacks of noisy labels in IA sequence segmentation.

All the unlabeled images can be labeled with a new teacher, i.e., the student from the previous stage, and re-trained in the

iterative training stage. Fig. 8 presents our examination of the effectiveness of iterative training in pST. In the extremely scarce-label regime with only one labeled sequence (#1), performance can be improved from 69.93% to 70.7% with the extra re-training stage. However, the performance of #10 decreased from 77.48% to 76.92% after re-training. This can be attributed to the fact that 10 labeled sequences are sufficient to train the best-learning model to produce reliable pseudo-labels. Iterative training introduces more noise, leading to performance degradation.

TABLE V
ABLATION RESEARCH RESULTS OF PST FOR SEMI-SUPERVISED IA SEQUENCE SEGMENTATION.

Methods	Data		Metrics						
	Labels	Unlabels	DSC	Acc	Sen	Spe	IOU	AUC	VC ↓
Teacher	1	0	66.89	94.32	68.89	96.39	51.41	90.18	129.49
Student	1	30	69.78	94.89	71.23	96.85	54.7	96.06	78.17
Student w/o SDA	1	60	68.39	94.77	68.91	96.89	53.06	95.1	84.50
Student	1	60	69.93	94.97	70.85	96.97	54.89	96.52	76.67
Teacher	3	0	74.35	95.84	77.61	97.39	59.51	96.78	80.51
Student	3	30	75.43	95.98	79.17	97.42	60.89	97.74	68.01
Student w/o SDA	3	60	75.09	95.99	77.73	97.54	60.46	97.32	65.88
Student	3	60	75.67	96.08	78.73	97.56	61.15	97.76	66.06
Teacher	10	0	76.66	96.4	76.96	98.12	62.4	98.21	61.91
Student	10	30	77.16	96.51	76.85	98.23	63.04	98.24	56.91
Student w/o SDA	10	60	77.07	96.51	76.62	98.25	62.92	98.16	56.11
Student	10	60	77.51	96.57	77.07	98.27	63.48	98.31	56.38

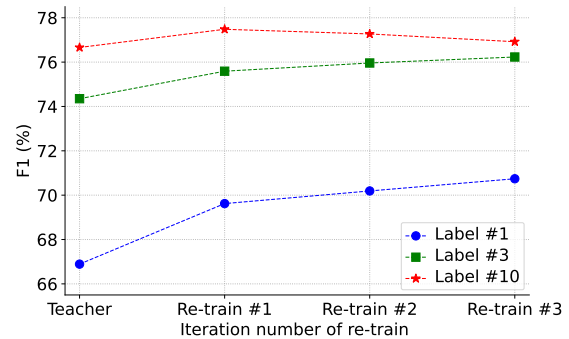


Fig. 8. Result of iterative training with different amounts of labeled data.

E. Impact of Model Input

The DSA sequence is a 2D temporal image sequence that represents the contrast agent’s response at different times while

flowing through the blood, and the collective response of all images results in accurate vessel delineation. We conduct comparative experiments that include subsets of the image sequence (First, Last, and First+Last) as input to the model to evaluate our hypothesis. Additionally, we apply averaging and minimizing operations on the entire sequence for each pixel in the sequence dimension to obtain minimum intensity projection (MIP) and average intensity projection (AIP) images. As shown in Table VI, segmentation results from ‘First’ that only highlights the ICA by the contrast agent exhibit poor performance. In comparison, the ‘Last’ as input to the model obtained better results, thanks to the more angiographic information in thin vessel.

The quantitative results are consistent with those portrayed in Fig. 9 (e) and (f). When using only the first image as the model input, the large vessels are accurately segmented, but the small vessels remain incomplete. On the other hand, using only the last image as an input results in the correct segmentation of most small vessels and some large ones. The combination of early and late arterial angiography, known as ‘First+Last’, yielded favorable results, surpassing those of both inputs used independently. The segmentation results of MIP and AIP are similar to those obtained using the method that utilizes the full DSA sequence as input, with the exception of Sen. The values for Sen are 75.72% and 75.44%, significantly lower than the value of 77.53% for the ‘Full’ method. The experimental findings indicate that employing the complete DSA sequence as input is imperative for achieving optimal performance.

TABLE VI
RESULTS OF FULLY-SUPERVISED SEGMENTATION WITH VARIOUS INPUT

Input	DSC	Acc	Sen	Spe	IOU	AUC
MIP	78.34	96.71	75.72	98.66	64.75	98.51
AIP	78.27	96.74	75.44	98.60	64.47	98.19
First image	61.93	95.13	52.98	98.68	45.74	90.12
Last image	76.23	96.53	72.86	98.61	61.73	98.20
First + Last image	77.51	96.70	74.24	98.69	63.38	98.46
Full	78.50	96.78	77.53	98.44	64.60	98.53

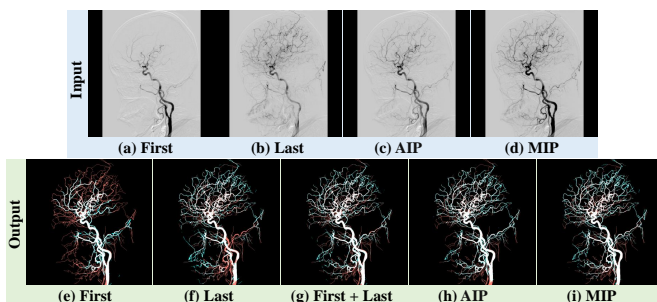


Fig. 9. The first row is the visualization of various inputs, and the second row is the corresponding segmentation result.

VI. CONCLUSION

In this paper, we introduce the DSA-sequence IA segmentation (DIAS) dataset, which includes pixel-level annotations

and two forms of weakly supervised annotations. We designed three benchmarks to evaluate the performance of IA sequence segmentation for DIAS. These include (1) the dimensionality reduction module combined with the 2D/3D model; (2) the scribble learning-based segmentation framework SSCR; and (3) the random patch-based self-training framework. With the constructed DIAS, we conduct a comprehensive experiments to demonstrate the effectiveness of the proposed methods, which enables insights into their performance and sheds light on future research. In the future, we will continue our research from the perspective of data, such as expanding segmentation targets to include venous vessels and segmenting arteries from complete angiographic sequences. The DIAS dataset and benchmark are publicly available for researchers to reproduce and explore new algorithms.

REFERENCES

- [1] C. P. Hess, “Imaging in cerebrovascular disease,” *Molecular, Genetic, and Cellular Advances in Cerebrovascular Diseases*, pp. 1–23, 2018.
- [2] S. Shaban, B. Huasen, A. Haridas, M. Killingsworth, J. Worthington, P. Jabbour, and S. M. M. Bhaskar, “Digital subtraction angiography in cerebrovascular disease: current practice and perspectives on diagnosis, acute treatment and prognosis,” *Acta Neurologica Belgica*, vol. 122, no. 3, pp. 763–780, 2022.
- [3] R. Su, S. A. Cornelissen, M. Van Der Sluijs, A. C. Van Es, W. H. Van Zwam, D. W. Dippel, G. Lycklama, P. J. Van Doormaal, W. J. Niessen, A. Van Der Lugt *et al.*, “autotici: Automatic brain tissue reperfusion scoring on 2d dsa images of acute ischemic stroke patients,” *IEEE Transactions on Medical Imaging*, vol. 40, no. 9, pp. 2380–2391, 2021.
- [4] M. Nielsen, M. Waldmann, T. Sentker, A. Frölich, J. Fiehler, and R. Werner, “Time matters: handling spatio-temporal perfusion information for automated tici scoring,” in *International Conference on Medical Image Computing and Computer-Assisted Intervention*. Springer, 2020, pp. 86–96.
- [5] M. Spiegel, T. Redel, T. Struffert, J. Hornegger, and A. Doerfler, “A 2d driven 3d vessel segmentation algorithm for 3d digital subtraction angiography data,” *Physics in Medicine & Biology*, vol. 56, no. 19, p. 6401, 2011.
- [6] U. Mitrović, B. Likar, F. Pernuš, and Ž. Špiclin, “3d–2d registration in endovascular image-guided surgery: Evaluation of state-of-the-art methods on cerebral angiograms,” *International journal of computer assisted radiology and surgery*, vol. 13, no. 2, pp. 193–202, 2018.
- [7] H. Jin, J. Geng, Y. Yin, M. Hu, G. Yang, S. Xiang, X. Zhang, Z. Ji, X. Fan, P. Hu *et al.*, “Fully automated intracranial aneurysm detection and segmentation from digital subtraction angiography series using an end-to-end spatiotemporal deep neural network,” *Journal of NeuroInterventional Surgery*, vol. 12, no. 10, pp. 1023–1027, 2020.
- [8] J. Zhang, G. Wang, H. Xie, S. Zhang, Z. Shi, and L. Gu, “Vesselness-constrained robust pca for vessel enhancement in x-ray coronary angiograms,” *Physics in Medicine & Biology*, vol. 63, no. 15, p. 155019, 2018.
- [9] N. Sang, H. Li, W. Peng, and T. Zhang, “Knowledge-based adaptive thresholding segmentation of digital subtraction angiography images,” *Image and Vision Computing*, vol. 25, no. 8, pp. 1263–1270, 2007.
- [10] B. Liu, Q. Jiang, W. Liu, M. Wang, S. Zhang, X. Zhang, B. Zhang, and Z. Yue, “A vessel segmentation method for serialized cerebralvascular dsa images based on spatial feature point set of rotating coordinate system,” *Computer Methods and Programs in Biomedicine*, vol. 161, pp. 55–72, 2018.
- [11] C. Meng, K. Sun, S. Guan, Q. Wang, R. Zong, and L. Liu, “Multiscale dense convolutional neural network for dsa cerebrovascular segmentation,” *Neurocomputing*, vol. 373, pp. 123–134, 2020.
- [12] R.-Q. Li, G.-B. Bian, X.-H. Zhou, X. Xie, Z.-L. Ni, and Z. Hou, “Cau-net: A novel convolutional neural network for coronary artery segmentation in digital subtraction angiography,” in *International Conference on Neural Information Processing*. Springer, 2020, pp. 185–196.
- [13] J. Staal, M. D. Abràmoff, M. Niemeijer, M. A. Viergever, and B. van Ginneken, “Ridge-based vessel segmentation in color images of the retina,” *IEEE Trans. Medical Imaging*, vol. 23, no. 4, pp. 501–509, 2004. [Online]. Available: <https://doi.org/10.1109/TMI.2004.825627>

- [14] M. M. Fraz, P. Remagnino, A. Hoppe, B. Uyyanonvara, A. R. Rudnicka, C. G. Owen, and S. A. Barman, "An ensemble classification-based approach applied to retinal blood vessel segmentation," *IEEE Transactions on Biomedical Engineering*, vol. 59, no. 9, pp. 2538–2548, Sep. 2012.
- [15] A. Hoover, V. Kouznetsova, and M. Goldbaum, "Locating blood vessels in retinal images by piecewise threshold probing of a matched filter response," *IEEE Transactions on Medical Imaging*, vol. 19, no. 3, pp. 203–210, 2000.
- [16] J. Odstrcilik, R. Kolar, A. Budai, J. Hornegger, J. Jan, J. Gazarek, T. Kubena, P. Cernosek, O. Svoboda, and E. Angelopoulou, "Retinal vessel segmentation by improved matched filtering: evaluation on a new high-resolution fundus image database," *IET Image Processing*, vol. 7, no. 4, pp. 373–383, 2013.
- [17] Y. Ma, H. Hao, J. Xie, H. Fu, J. Zhang, J. Yang, Z. Wang, J. Liu, Y. Zheng, and Y. Zhao, "Rose: a retinal oct-angiography vessel segmentation dataset and new model," *IEEE transactions on medical imaging*, vol. 40, no. 3, pp. 928–939, 2020.
- [18] A. Carballal, F. J. Nóvoa, C. Fernandez-Lozano, M. García-Guimaraes, G. López-Campos, R. Calviño-Santos, J. M. Vázquez-Naya, and A. Pazos, "Automatic multiscale vascular image segmentation algorithm for coronary angiography," *Biomed. Signal Process. Control.*, vol. 46, pp. 1–9, 2018. [Online]. Available: <https://doi.org/10.1016/j.bspc.2018.06.007>
- [19] F. Cervantes-Sanchez, I. Cruz-Aceves, A. Hernandez-Aguirre, M. A. Hernandez-Gonzalez, and S. E. Solorio-Meza, "Automatic Segmentation of Coronary Arteries in X-ray Angiograms using Multiscale Analysis and Artificial Neural Networks," *Applied Sciences*, vol. 9, no. 24, 2019. [Online]. Available: <https://www.mdpi.com/2076-3417/9/24/5507>
- [20] R. Gharleghi, D. Adikari, K. Ellenberger, S.-Y. Ooi, C. Ellis, C.-M. Chen, R. Gao, Y. He, R. Hussain, C.-Y. Lee *et al.*, "Automated segmentation of normal and diseased coronary arteries—the asoca challenge," *Computerized Medical Imaging and Graphics*, vol. 97, p. 102049, 2022.
- [21] R. D. Rudyanto, S. Kerkstra, E. M. Van Rikxoort, C. Fetita, P.-Y. Brilllet, C. Lefevre, W. Xue, X. Zhu, J. Liang, I. Öksüz *et al.*, "Comparing algorithms for automated vessel segmentation in computed tomography scans of the lung: the vessel12 study," *Medical image analysis*, vol. 18, no. 7, pp. 1217–1232, 2014.
- [22] M. Zhang, F. Yu, J. Zhao, L. Zhang, and Q. Li, "Befd: boundary enhancement and feature denoising for vessel segmentation," in *International Conference on Medical Image Computing and Computer-Assisted Intervention*. Springer, 2020, pp. 775–785.
- [23] O. Ronneberger, P. Fischer, and T. Brox, "U-net: Convolutional networks for biomedical image segmentation," in *International Conference on Medical image computing and computer-assisted intervention*. Springer, 2015, pp. 234–241.
- [24] D. Jia and X. Zhuang, "Learning-based algorithms for vessel tracking: A review," *Computerized Medical Imaging and Graphics*, vol. 89, p. 101840, 2021.
- [25] W. Liu, H. Yang, T. Tian, X. Pan, and W. Xu, "Multiscale attention aggregation network for 2d vessel segmentation," in *ICASSP 2022-2022 IEEE International Conference on Acoustics, Speech and Signal Processing (ICASSP)*. IEEE, 2022, pp. 1436–1440.
- [26] H. Wu, W. Wang, J. Zhong, B. Lei, Z. Wen, and J. Qin, "Scs-net: A scale and context sensitive network for retinal vessel segmentation," *Medical Image Analysis*, vol. 70, p. 102025, 2021.
- [27] Y. Wu, Y. Xia, Y. Song, D. Zhang, D. Liu, C. Zhang, and W. Cai, "Vessel-net: Retinal vessel segmentation under multi-path supervision," in *International conference on medical image computing and computer-assisted intervention*. Springer, 2019, pp. 264–272.
- [28] W. Liu, H. Yang, T. Tian, Z. Cao, X. Pan, W. Xu, Y. Jin, and F. Gao, "Full-resolution network and dual-threshold iteration for retinal vessel and coronary angiograph segmentation," *IEEE Journal of Biomedical and Health Informatics*, vol. 26, no. 9, pp. 4623–4634, 2022.
- [29] L. Mou, Y. Zhao, H. Fu, Y. Liu, J. Cheng, Y. Zheng, P. Su, J. Yang, L. Chen, A. F. Frangi *et al.*, "Cs2-net: Deep learning segmentation of curvilinear structures in medical imaging," *Medical image analysis*, vol. 67, p. 101874, 2021.
- [30] S. Zhang, H. Fu, Y. Yan, Y. Zhang, Q. Wu, M. Yang, M. Tan, and Y. Xu, "Attention guided network for retinal image segmentation," in *International conference on medical image computing and computer-assisted intervention*. Springer, 2019, pp. 797–805.
- [31] W. Wang, J. Zhong, H. Wu, Z. Wen, and J. Qin, "Rvseg-net: An efficient feature pyramid cascade network for retinal vessel segmentation," in *International Conference on Medical Image Computing and Computer-Assisted Intervention*. Springer, 2020, pp. 796–805.
- [32] S. A. Kamran, K. F. Hossain, A. Tavakkoli, S. L. Zuckerbrod, K. M. Sanders, and S. A. Baker, "Rv-gan: segmenting retinal vascular structure in fundus photographs using a novel multi-scale generative adversarial network," in *International Conference on Medical Image Computing and Computer-Assisted Intervention*. Springer, 2021, pp. 34–44.
- [33] S. Y. Shin, S. Lee, I. D. Yun, and K. M. Lee, "Deep vessel segmentation by learning graphical connectivity," *Medical image analysis*, vol. 58, p. 101556, 2019.
- [34] Y. Zhou, H. Yu, and H. Shi, "Study group learning: Improving retinal vessel segmentation trained with noisy labels," in *International Conference on Medical Image Computing and Computer-Assisted Intervention*. Springer, 2021, pp. 57–67.
- [35] R. Xu, T. Liu, X. Ye, L. Lin, and Y.-W. Chen, "Boosting connectivity in retinal vessel segmentation via a recursive semantics-guided network," in *International Conference on Medical Image Computing and Computer-Assisted Intervention*. Springer, 2020, pp. 786–795.
- [36] H. Zhao, H. Li, and L. Cheng, "Improving retinal vessel segmentation with joint local loss by matting," *Pattern Recognition*, vol. 98, p. 107068, 2020.
- [37] M. Tang, F. Perazzi, A. Djelouah, I. Ben Ayed, C. Schroers, and Y. Boykov, "On regularized losses for weakly-supervised cnn segmentation," in *Proceedings of the European Conference on Computer Vision (ECCV)*, 2018, pp. 507–522.
- [38] X. Luo, W. Liao, J. Xiao, J. Chen, T. Song, X. Zhang, K. Li, D. N. Metaxas, G. Wang, and S. Zhang, "Word: A large scale dataset, benchmark and clinical applicable study for abdominal organ segmentation from ct image," *Medical Image Analysis*, vol. 82, p. 102642, 2022.
- [39] D. Lachinov, P. Seeböck, J. Mai, F. Goldbach, U. Schmidt-Erfurth, and H. Bognovic, "Projective skip-connections for segmentation along a subset of dimensions in retinal oct," in *International Conference on Medical Image Computing and Computer-Assisted Intervention*. Springer, 2021, pp. 431–441.
- [40] M. Li, Y. Chen, Z. Ji, K. Xie, S. Yuan, Q. Chen, and S. Li, "Image projection network: 3d to 2d image segmentation in octa images," *IEEE Transactions on Medical Imaging*, vol. 39, no. 11, pp. 3343–3354, 2020.
- [41] W. Liu, H. Yang, T. Tian, Z. Cao, X. Pan, W. Xu, Y. Jin, and F. Gao, "Full-resolution network and dual-threshold iteration for retinal vessel and coronary angiograph segmentation," *IEEE Journal of Biomedical and Health Informatics*, vol. 26, no. 9, pp. 4623–4634, 2022.
- [42] W. Liu, T. Tian, W. Xu, H. Yang, X. Pan, S. Yan, and L. Wang, "Phtrans: Parallely aggregating global and local representations for medical image segmentation," in *Medical Image Computing and Computer Assisted Intervention—MICCAI 2022: 25th International Conference, Singapore, September 18–22, 2022, Proceedings, Part V*. Springer, 2022, pp. 235–244.
- [43] X. Chen, Y. Yuan, G. Zeng, and J. Wang, "Semi-supervised semantic segmentation with cross pseudo supervision," in *Proceedings of the IEEE/CVF Conference on Computer Vision and Pattern Recognition*, 2021, pp. 2613–2622.
- [44] W. Liu, W. Xu, S. Yan, L. Wang, H. Li, and H. Yang, "Combining self-training and hybrid architecture for semi-supervised abdominal organ segmentation," in *Fast and Low-Resource Semi-supervised Abdominal Organ Segmentation: MICCAI 2022 Challenge, FLARE 2022, Held in Conjunction with MICCAI 2022, Singapore, September 22, 2022, Proceedings*. Springer, 2023, pp. 281–292.
- [45] D.-H. Lee *et al.*, "Pseudo-label: The simple and efficient semi-supervised learning method for deep neural networks," in *Workshop on challenges in representation learning, ICML*, vol. 3, no. 2, 2013, p. 896.
- [46] L. Yang, W. Zhuo, L. Qi, Y. Shi, and Y. Gao, "St++: Make self-training work better for semi-supervised semantic segmentation," in *Proceedings of the IEEE/CVF Conference on Computer Vision and Pattern Recognition*, 2022, pp. 4268–4277.
- [47] I. Loshchilov and F. Hutter, "Decoupled weight decay regularization," *arXiv preprint arXiv:1711.05101*, 2017.
- [48] J. Schlemper, O. Oktay, M. Schaap, M. Heinrich, B. Kainz, B. Glocker, and D. Rueckert, "Attention gated networks: Learning to leverage salient regions in medical images," *Medical image analysis*, vol. 53, pp. 197–207, 2019.
- [49] Z. Zhou, M. M. Rahman Siddiquee, N. Tajbakhsh, and J. Liang, "Unet++: A nested u-net architecture for medical image segmentation," in *Deep learning in medical image analysis and multimodal learning for clinical decision support*. Springer, 2018, pp. 3–11.
- [50] X. Xiao, S. Lian, Z. Luo, and S. Li, "Weighted res-unet for high-quality retina vessel segmentation," in *2018 9th international conference on information technology in medicine and education (ITME)*. IEEE, 2018, pp. 327–331.
- [51] M. Tang, A. Djelouah, F. Perazzi, Y. Boykov, and C. Schroers, "Normalized cut loss for weakly-supervised cnn segmentation," in *Proceedings*

of the IEEE conference on computer vision and pattern recognition, 2018, pp. 1818–1827.

- [52] Y. Grandvalet and Y. Bengio, “Semi-supervised learning by entropy minimization,” *Advances in neural information processing systems*, vol. 17, 2004.